

# Localized Forcing on Thin Liquid Films

Edwin Lei

May 20, 2008

## 1 Introduction

### 1.1 Overview

Many industrial processes involve applying a uniform thin coat of fluid to a solid surface. One possible technique is to use a laser to adjust the height of the thin film on an inclined plane that is subject to the gravitational force and the Marangoni force. This paper studied the long term dynamics of the height of the thin film. In general, the Marangoni force is a result of differences in surface tension. This difference in surface tension is induced by a temperature gradient applied to the inclined plane. The bottom of the plane is warmer, so the surface tension is lower. On the other hand, the top of the plane is cooler, so the surface tension is higher. The thin fluid will therefore creep toward the higher surface tension region. A description of the experimental setup is in Section 1.2. A brief explanation on the derivation of the partial differential equation (PDE) that models the thin film's behavior is given in Section 1.3. Next, from linear stability analysis, section 2 describes the stability of equilibria points of an ODE simplification to the PDE model. Section 3 describes two other approaches to the same problem which also yield identical results. Finally, in Section 4, we will numerically construct the phase portrait of the steady-state solution called the Poincaré map. This graphical representation will indirectly allow us to obtain the solution to the simplified ODE model.

### 1.2 Experimental Setup

A diagram of the experimental setup is shown in Figure 1, where  $g$  is the acceleration due to gravity,  $\tau$  is a constant temperature gradient different from the laser that draws the fluid up the inclined plane,  $\alpha$  is the plane's inclination angle,  $h_0$  is the film's initial height,  $h_U$  is the upstream height, and  $h_D$  is the downstream height. The temperature gradient  $\tau$ , the Marangoni force, induces a difference in surface tension. When this force exceeds the downward force of gravity, the film moves up the inclined plane.

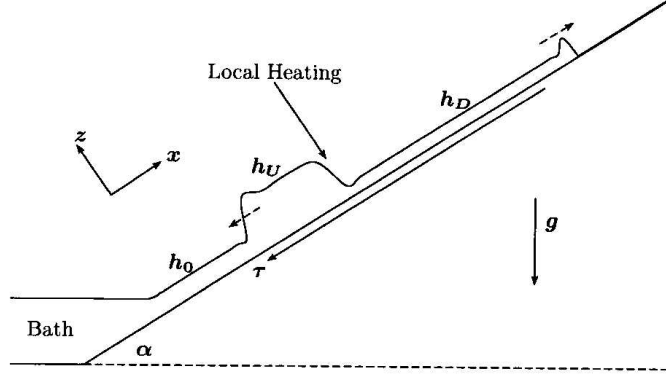


Figure 1: Schematic diagram of the experimental setup (Source: [2]).

### 1.3 Differential Equation Model

If we model the localized forcing of the laser as a Gaussian centered at  $x = 0$ ,  $\theta(x) = \left(\frac{1}{\sqrt{2\pi}}\right) e^{-\frac{x^2}{2}}$ , then

$$\frac{\partial h}{\partial t} + \frac{\partial}{\partial x}(h^2 - h^3) = M \frac{\partial}{\partial x} \left( h^2 \frac{d\theta}{dx} \right) - \frac{\partial}{\partial x} \left( h^3 \frac{\partial^3 h}{\partial x^3} \right), \quad (1)$$

describes the change in the thin film's height over time and space where  $h$  is the film height and  $M$  is the nondimensionalized forcing coefficient. Note that  $f(h) = h^2 - h^3$  models the competing effects of gravity ( $h^3$ ) and Marangoni ( $h^2$ ) forces. PDE (1) can be derived using the well-known lubrication approximation and a depth-averaged velocity [1]. Since we are interested in the long-term behavior of the film, it is therefore appropriate to look at the steady-state solution of (1). These steady-state solutions satisfy the ordinary differential equation

$$\frac{d}{dx} (h^2 - h^3) = M \frac{d}{dx} \left( h^2 \frac{d\theta}{dx} \right) - \frac{d}{dx} \left( h^3 \frac{d^3 h}{dx^3} \right). \quad (2)$$

Integrating ODE (2) gives

$$h^2 - h^3 = M h^2 \frac{d\theta}{dx} - h^3 \frac{d^3 h}{dx^3} + C, \quad (3)$$

where  $C$  is a constant of integration. To solve for  $C$ , we further assume that in steady-state, bounded solutions for  $h(x)$  of ODE (3) are sufficiently far away from the forcing  $\theta(x)$ . Since  $\theta(x) \rightarrow 0$  for large  $|x|$ , bounded solutions to ODE (3) must approach  $h_U$  for  $x \rightarrow -\infty$  and  $h_D$  for  $x \rightarrow \infty$ . Hence,  $C = h_U^2 - h_U^3 = h_D^2 - h_D^3$ , and without loss of generality, assume  $C = h_U^2 - h_U^3$ . ODE (3) therefore becomes

$$\frac{d^3 h}{dx^3} = \frac{1}{h^3} \left( M h^2 \frac{d\theta}{dx} - h^2 + h^3 + h_U^2 - h_U^3 \right). \quad (4)$$

To analyze solutions to ODE (4), we will use a dynamical systems approach to understand the stability of equilibria.

## 2 Linear Stability Analysis

We write ODE (4) as an equivalent system of three first order differential equations

$$\begin{bmatrix} h' \\ u' \\ v' \end{bmatrix} = \begin{bmatrix} u \\ v \\ \frac{1}{h^3} (Mh^2 \frac{d\theta}{dx} - h^2 + h^3 + h_U^2 - h_U^3) \end{bmatrix} \quad (5)$$

To find equilibria of system (5), we will again make the approximation that  $\theta(x) \rightarrow 0$  at far downstream and far upstream heights  $h_D$  and  $h_U$ . Solving  $h' = u' = v' = 0$  gives three equilibria

$$[\vec{h}_1^*, \vec{h}_2^*, \vec{h}_3^*] = \left[ \begin{bmatrix} h_1 \\ 0 \\ 0 \end{bmatrix}, \begin{bmatrix} h_2 \\ 0 \\ 0 \end{bmatrix}, \begin{bmatrix} h_3 \\ 0 \\ 0 \end{bmatrix} \right], \quad (6)$$

where

$$h_1 = h_U \quad (7a)$$

$$h_2 = \frac{1}{2} \left( 1 - h_U + \sqrt{1 + 2h_U - 3h_U^2} \right) \quad (7b)$$

$$h_3 = \frac{1}{2} \left( 1 - h_U - \sqrt{1 + 2h_U - 3h_U^2} \right). \quad (7c)$$

Since  $h_3 \leq 0$  for  $h_U \in [0, 1]$ ,  $\vec{h}_3^*$  is unphysical and we discard it from our analysis.

To analyze the fixed points' stability, we will calculate the Jacobian matrix with the assumption that  $M$ , the local forcing parameter, is small. This approximation allows us to ignore the  $Mh^2 \frac{d\theta}{dx}$  term even at  $\vec{h}_2^*$ , which is not faraway from  $x = 0$ . Evaluated at  $\vec{h}_1^*$  and  $\vec{h}_2^*$ , respectively, the matrix is

$$\begin{bmatrix} 0 & 1 & 0 \\ 0 & 0 & 1 \\ \frac{1}{(h_1)^4} ((h_1)^2 - 3h_U^2 + 3h_U^3) & 0 & 0 \end{bmatrix} \quad (8a)$$

$$\begin{bmatrix} 0 & 1 & 0 \\ 0 & 0 & 1 \\ \frac{1}{(h_2)^4} ((h_2)^2 - 3h_U^2 + 3h_U^3) & 0 & 0 \end{bmatrix}. \quad (8b)$$

The eigenvalues of matrix (8a) are

$$\begin{bmatrix} \lambda_{11} \\ \lambda_{12} \\ \lambda_{13} \end{bmatrix} = \begin{bmatrix} 2a \\ -a + a\sqrt{3}i \\ -a - a\sqrt{3}i \end{bmatrix}, \quad (9)$$

where  $a = \frac{(3h_U^2 - 2h_U)^{\frac{1}{3}}}{2h_U}$ . The corresponding eigenvectors are

$$[\vec{v}_{11}, \vec{v}_{12}, \vec{v}_{13}] = \left[ \begin{bmatrix} 1 \\ \lambda_{11} \\ \lambda_{11}^2 \end{bmatrix}, \begin{bmatrix} 1 \\ \lambda_{12} \\ \lambda_{12}^2 \end{bmatrix}, \begin{bmatrix} 1 \\ \lambda_{13} \\ \lambda_{13}^2 \end{bmatrix} \right]. \quad (10)$$

Similarly, the eigenvalues of matrix (8b) are

$$\begin{bmatrix} \lambda_{21} \\ \lambda_{22} \\ \lambda_{23} \end{bmatrix} = \begin{bmatrix} 2b \\ -b + b\sqrt{3}i \\ -b - b\sqrt{3}i \end{bmatrix}, \quad (11)$$

where  $b = \frac{1}{2} \left( \frac{2 - 3h_U^2 + 5h_U - 3h_U \sqrt{1 + 2h_U - 3h_U^2} - 2\sqrt{1 + 2h_U - 3h_U^2}}{2h_U^3 - 2h_U^2} \right)^{\frac{1}{3}}$ . The corresponding eigenvectors are

$$[\vec{v}_{21}, \vec{v}_{22}, \vec{v}_{23}] = \left[ \begin{bmatrix} 1 \\ \lambda_{21} \\ \lambda_{21}^2 \end{bmatrix}, \begin{bmatrix} 1 \\ \lambda_{22} \\ \lambda_{22}^2 \end{bmatrix}, \begin{bmatrix} 1 \\ \lambda_{23} \\ \lambda_{23}^2 \end{bmatrix} \right]. \quad (12)$$

## 2.1 Solution Trajectories

The one-dimensional solution trajectory about fixed point  $\vec{h}_1^* = [h_U \ 0 \ 0]^T$  is

$$A \begin{bmatrix} 1 \\ 2a \\ 4a^2 \end{bmatrix} e^{2ax}, \quad (13)$$

for any constant  $A$ . Similarly, the two-dimensional trajectory is

$$B e^{-ax} p(x) + C e^{-ax} q(x), \quad (14)$$

where  $B$  and  $C$  are constants,  $p(x)$  is

$$\begin{bmatrix} 1 \\ -a \\ -a^2 \end{bmatrix} \cos(a\sqrt{3}x) - \begin{bmatrix} 0 \\ a\sqrt{3} \\ -2a^2\sqrt{3} \end{bmatrix} \sin(a\sqrt{3}x), \quad (15)$$

and  $q(x)$  is

$$\begin{bmatrix} 1 \\ -a \\ -a^2 \end{bmatrix} \sin(a\sqrt{3}x) + \begin{bmatrix} 0 \\ a\sqrt{3} \\ -2a^2\sqrt{3} \end{bmatrix} \cos(a\sqrt{3}x). \quad (16)$$

This result can be derived by recognizing  $\vec{v}_{12}$  is a complex-valued vector (since  $\lambda_{12}$  is complex-valued) and then decomposing  $\vec{v}_{12}$  into its real and imaginary parts. Furthermore, since  $\vec{v}_{12}$  and  $\vec{v}_{13}$  are complex conjugates, the latter does not provide additional information to the two-dimensional trajectory (14).

Similar calculations to (13) and (14) will give the one-dimensional solution trajectory about fixed point  $\vec{h}_2^* = \left[ \frac{1}{2} \left( 1 - h_U + \sqrt{1 + 2h_U - 3h_U^2} \right) \quad 0 \quad 0 \right]^T$

$$D \begin{bmatrix} 1 \\ 2b \\ 4b^2 \end{bmatrix} e^{2bx}, \quad (17)$$

for any constant  $D$ . The two-dimensional trajectory is

$$E e^{-bx} r(x) + F e^{-bx} s(x), \quad (18)$$

where  $E$  and  $F$  are constants,  $r(x)$  is

$$\begin{bmatrix} 1 \\ -b \\ -b^2 \end{bmatrix} \cos(b\sqrt{3}x) - \begin{bmatrix} 0 \\ b\sqrt{3} \\ -2b^2\sqrt{3} \end{bmatrix} \sin(b\sqrt{3}x), \quad (19)$$

and  $s(x)$  is

$$\begin{bmatrix} 1 \\ -b \\ -b^2 \end{bmatrix} \sin(b\sqrt{3}x) + \begin{bmatrix} 0 \\ b\sqrt{3} \\ -2b^2\sqrt{3} \end{bmatrix} \cos(b\sqrt{3}x). \quad (20)$$

For  $0 < h_U < \frac{2}{3}$ ,  $a < 0$  implies  $\lambda_{11} < 0$  and  $\text{Re}[\lambda_{12}] = \text{Re}[\lambda_{13}] > 0$ . In other words, trajectory (13) refers to a stable node, and trajectory (14) refers to an unstable spiral. For this same range of  $h_U$ ,  $b > 0$  implies  $\lambda_{21} > 0$  and  $\text{Re}[\lambda_{22}] = \text{Re}[\lambda_{23}] < 0$ . Hence, trajectory (17) refers to an unstable node and trajectory (18) refers to a stable spiral.

A numerical solution to PDE (1) shown in Figure 2 confirms our results. For  $h_0 = 0.4$ , the one-dimensional trajectory (13) predicts  $\vec{h}_1^* = [h_U \quad 0 \quad 0]^T = [h_D \quad 0 \quad 0]^T = [0.4 \quad 0 \quad 0]^T$  to be a stable node, which is verified by points 1 and 5 labeled on Figure 2. Furthermore, the dips between points 1 and 2 and points 4 and 5 correspond to the unstable spiral predicted by trajectory (14). Furthermore, the unstable node predicted by trajectory (17) corresponds to point 3 on Figure 2. When  $h_0 = 0.4$ , equation (7b) gives  $h_2 = 0.88$ , as shown in the figure.

If we imagine the thin film traveling from  $x = -\infty$  to  $x = \infty$  forward in time, the film first leaves point 1 on Figure 2 on an unstable two-dimensional manifold according to trajectory (14). Then it oscillates around the fixed point  $\vec{h}_2^* = [0.88 \quad 0 \quad 0]^T$  on a stable two-dimensional manifold according to trajectory (18). However, the thin film then moves away from  $\vec{h}_2^*$  on a one-dimensional unstable manifold according to trajectory (17). Finally, it approaches fixed point  $\vec{h}_1^*$  on a two-dimensional manifold according to trajectory (14) and

subsequently settles down at  $\vec{h}_1^*$  with height  $h = 0.4$  on a one-dimensional stable manifold, shown as point 5 on Figure 2. Since the thin film started from and returned to  $\vec{h}_1^*$ , we say the solution trajectory followed a homoclinic orbit from  $\vec{h}_1^*$  to itself.

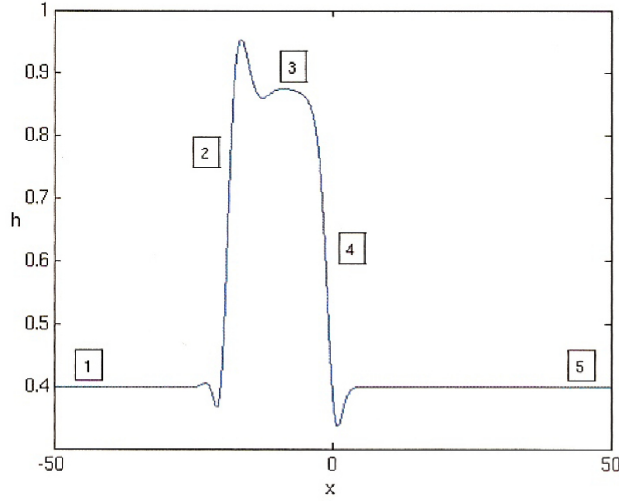


Figure 2: PDE simulation of the steady-state solution for small values of  $M$  (Source:[2]).

Furthermore, only when  $0 < h_U < \frac{2}{3}$  is  $\lambda_{11} < 0$  and  $\lambda_{21} > 0$ . When  $h_U > \frac{2}{3}$ ,  $\lambda_{11} > 0$  and  $\lambda_{21} < 0$ . As a result, we would expect a bifurcation to occur at  $h = \frac{2}{3}$ . It can be shown that for larger values of the forcing parameter  $M$  the change in stability can be realized.

### 3 Alternative Approaches

#### 3.1 Traveling Wave Solution

Instead of simplifying PDE (1) to a steady-state ODE, Levy [2] looked for traveling wave solutions to PDE (1). For a traveling wave,  $h(x, t) = h(x - st) = h(\xi)$ , solution of PDE (1), it can be shown that it satisfies

$$\frac{d^3 h}{d\xi^3} = \frac{1}{h^3} \left( Mh^2 \frac{d\theta}{d\xi} + sh - h^2 + h^3 - sh_U + h_U^2 - h_U^3 \right), \quad (21)$$

where  $s$  is the speed of the wave. A dynamical systems approach as in Section 2 would follow to analyze the stability of equilibria.

#### 3.2 Conservation of Flux

Haskett et al. [1] showed that, with or without forcing, to conserve mass globally, the fluxes upstream and downstream must balance,

$$h_U^2 - h_U^3 = h_D^2 - h_D^3. \quad (22)$$

Without loss of generality, solving equation (22) for  $h_D$  gives three roots, one of which is negative and hence unphysical. The other two roots correspond to two classes of solutions. The first class of solutions

$$h_D = h_U = h_0, \quad (23)$$

for any initial height  $h_0$ , is called Type I solutions. Haskett et al. calls the second class of solutions

$$h_D = \frac{1}{2} \left( 1 - h_U + \sqrt{1 + 2h_U - 3h_U^2} \right) \quad (24)$$

Type II solutions. Haskett et al. showed that Type I solutions correspond to weak forcing  $M$ , and Type II solutions correspond to forcing for some  $M > M_c$ , where  $M_c$  is the critical forcing value for which a bifurcation between the two classes of solutions occur.

Note that the results in Section 2 using linear stability analysis match those of Haskett et al. using a conservation argument.

## 4 Numerical Results

The results provided by Section 2 using linear stability analysis are only valid locally around the respective equilibria. To fully describe the evolution of a thin film's height would require solving the nonlinear third-order ODE (4), which may not be possible. An easier approach is to calculate phase space trajectories around the two equilibria points and then intersect their trajectories. At the point of intersection in phase space, the trajectories have the same  $h$ ,  $h'$ , and  $h''$ .

To explore this numerical approach more fully, we opt to use a simpler thin film on an inclined plane model that does not have local forcing and a temperature gradient. A derivation of the PDE model can be found in Levy and Shearer [3]. A traveling wave solution to the PDE yields a system of three first-order ODEs

$$\begin{bmatrix} h' \\ u' \\ v' \end{bmatrix} = \begin{bmatrix} u \\ v \\ \frac{1}{\kappa h^3} (3sh - h^3 + \beta h^3 u - 3k_h) \end{bmatrix}, \quad (25)$$

where  $\beta$  is related to the normal component of gravity,  $\kappa$  describes the surface tension of the thin film,  $k_h = \frac{1}{3}h_U h_D (h_U + h_D)$  is a constant of integration, and  $s = \frac{1}{3}(h_U^2 + h_U h_D + h_D^2)$  is the speed of the wave. Levy and Shearer showed that there are two equilibria points, one stable and the other unstable. In fact, the stability of the equilibria are the same as our original model's, which provides further justification for using a simpler model to explore the numerical approach. Figure 3 shows the MATLAB results for  $h_D = 0.7$ ,  $h_U = 0.3$ , and a very small perturbation away from each equilibrium point. In Figure 3(a), the red trajectory represents the unstable equilibrium, while the blue trajectory represents the stable equilibrium. We can see that the trajectories failed to intersect in phase space. As a result, the height profile of the thin film will therefore be discontinuous and unphysical, as shown in Figure 3(b). This brute force guess-and-check method was overly dependent on our checking to determine whether the trajectories actually crossed.

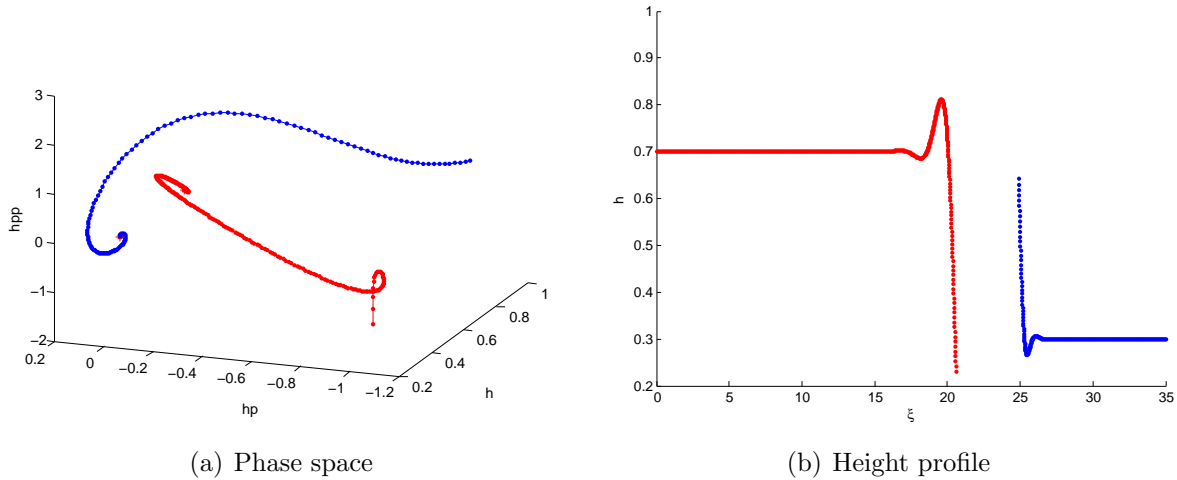


Figure 3: The trajectories do not intersect in phase space, which leads to a discontinuous height profile.

We used MATLAB's event location function to approach the problem more systematically. By choosing a height  $h$ , the event location function calculated  $h'$  and  $h''$  for both the stable and unstable trajectories at the specified height. Iterating this process produced a family of trajectories that cross the specified height of  $h = 0.5$ , but with different  $h'$  and  $h''$ . The result is called a Poincaré map and is shown in Figure 4. Each blue and red point on Figure 4 corresponds to a trajectory from the stable and unstable equilibrium crossing height  $h = 0.5$ , respectively. The point of intersection in Figure 4 between the red and blue curves corresponds to two trajectories having the same height  $h = 0.5$ ,  $h'$  and  $h''$ . This means a height profile similar to that of Figure 3(b) of these two trajectories will produce a continuous curve.

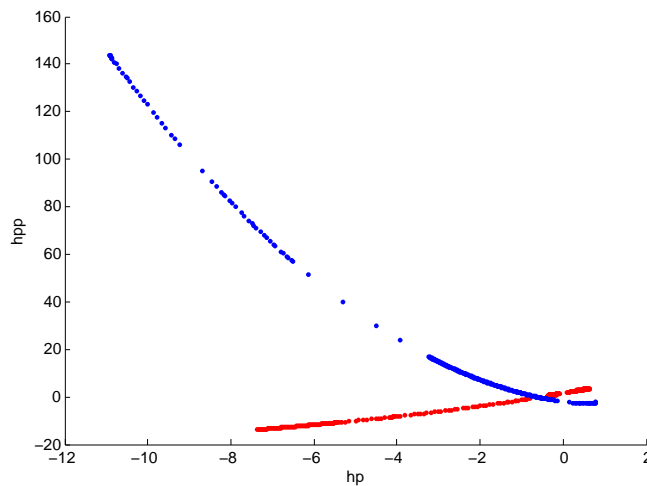


Figure 4: A Poincaré map showing the intersection of two trajectories at  $h = 0.5$ .

## 5 Conclusion

The next step in the numerical analysis is to re-incorporate our ODE model (4). The difficulty is that the  $\frac{d\theta}{dx}$  term in ODE (4) is a function of  $x$ , so it needs to be updated at every instance when we numerically solve the ODE using MATLAB. Nevertheless, we have shown that the Poincaré map is useful in identifying intersecting trajectories in phase space. This intersection corresponds to a physical and continuous height profile of the thin film.

## Acknowledgements

I would like to thank Professor Levy and Steve Rosenthal for the many hours they spent working on the problem with me. Also, I would like to thank Professor Yong for helping with MATLAB's event location function.

## References

- [1] Ryan P. Haskett, Thomas P. Witelski, and Jeanman Sur. Localized marangoni forcing in driven thin films. *Physica D: Nonlinear Phenomena*, 209(1-4):117–134, 9/15 2005.
- [2] Rachel Levy. Effects of localized forcing on driven thin liquid films. pages 177–186, 5 2006.
- [3] Rachel Levy and Michael Shearer. Comparison of two dynamic contact line models for driven thin liquid films. *European Journal of Applied Mathematics*, 15:625–642, 2004.